Impact of Wind Generation on Power Swing Protection

Aboutaleb Haddadi, *Member, IEEE,* Ilhan Kocar, *Senior Member, IEEE,* Ulas Karaagac, *Member, IEEE,* Henry Gras, and Evangelos Farantatos, *Senior Member, IEEE*

***Abstract*— Large-scale integration of wind generation changes the power swing characteristics of a power system and may result in the misoperation of legacy power swing protection schemes. This paper presents a qualitative study on the impact of wind generation on power swing protection. The objective is to provide an understanding of the problem through case studies and present possible solutions and adjustments in protection schemes to ensure the efficiency of protection under large-scale integration of wind generation. The misoperation of power swing protection functions, namely Power Swing Blocking (PSB) and Out-of-Step Tripping (OST), as a result of increased wind generation levels, are shown through case studies. It is also shown that the electrical center of a power system may move due to wind generation. In this case, it would be necessary to revise the optimal location of the OST protection. Finally, the impact of various factors such as wind generator type, control scheme and Fault-Ride-Through (FRT) function, and wind generation level and capacity are investigated to determine the key features that need to be accounted for in practical protection studies.**

***Index Terms*—Power system protection, Wind energy integration, Power swing protection, Power system faults, Power system simulation**

I. Introduction

Power swing is a temporal variation in the three-phase power flow caused by power system disturbances such as line switching, generator disconnection, and the loss or connection of large blocks of load [1]-[4]. A power swing may be stable, if the system regains a new state of equilibrium within acceptable operating boundaries, or unstable, if the system loses synchronism. During a power swing, the rotor angles of machines advance or retard relative to each other resulting in the variation of system voltages and currents. Protection devices which measure these quantities may interpret such transient variations as a system fault and mistakenly trip needed equipment. With regard to line distance protection, such a misoperation may occur when the swing impedance trajectory enters the operation zone of a line distance relay causing unintentional tripping of the line. This can further aggravate system's stability and possibly result in cascading outages and shutdown of major portions of the power system [1]-[2]. Power swing protection protects a power system against such malfunctions. Its philosophy is twofold: (i) avoid unintentional tripping of any power system equipment during a stable power swing to allow the system to return to a new equilibrium and (ii) protect the power system during an unstable or out-of-step (OOS) condition through a controlled separation of the system at predetermined locations to prevent widespread power outage and equipment damage. A power swing protection accomplishes these objectives through Power Swing Blocking (PSB) and Out-of-step Tripping (OST) functions; the PSB distinguishes between a fault and a power swing by measuring the rate of change of impedance vector and blocks the distance relay elements operation in case of a power swing; the OST differentiates between a stable and an unstable swing based on the swing impedance trajectory and initiates system partitioning in case of an unstable swing.

Inverter based resources including wind generation, have fault response characteristics that differ from traditional synchronous rotating generation and mainly depend on their converter control scheme [5]-[8]. Given that, the impact of inverter-based resources on bulk system protection has recently gained the interest of the power systems community [5] and the performance of various legacy protection schemes including distance protection [9]-[13] and negative sequence-based protection schemes has been recently studied [5],[14]-[15]. Another legacy protection scheme that is expected to be affected by large integration of wind generation is power swing protection, which is studied in this paper. Wind generation can considerably alter power swing characteristics [16]-[18] and may result in misoperation of the PSB and OST functions [5]. Faster power swings under wind generation, which are due to reduced system inertia [16]-[18], may not be detected by the PSB function and lead to PSB misoperation. A high share of wind generation also changes the swing impedance trajectory which may result in OST malfunction and unwanted system partitioning during a stable power swing. Further, the electrical center (EC) of a power system may move as wind generation level increases which changes the optimal location for the implementation of the OST protection [1],[2]. Thus, it is necessary to study these impacts and provide solutions to ensure an efficient protection under high levels of wind generation. So far, no paper in the literature has addressed this problem.

This paper studies the possible negative impacts of wind

A. Haddadi, I. Kocar, and H. Gras are with Montreal Polytechnique, Montreal, QC H3T1J4 Canada (e-mail: aboutaleb.haddadi@polymtl.ca ilhan.kocar@polymtl.ca henry.gras@polymtl.ca).

U. Karaagac is with the Hong Kong Polytechnic University, Hung Hom, Kowloon, Hong Kong (e-mail: ulas.karaagac@polymtl.ca).

Evangelos Farantatos is with the Electric Power Research Institute (EPRI), Palo Alto, CA (e-mail: efarantatos@epri.com).

generation on power swing protection. As [2] has pointed out, this is a complex problem, and it is difficult to address it analytically in general. This paper presents a qualitative study whose objective is to provide an understanding of the problem through case studies and propose possible solutions and adjustments in protection schemes to ensure the efficiency of protection under high levels of wind generation. Specifically, this paper provides examples of PSB and OST malfunction and the movement of EC due to wind generation. The paper further illustrates the impact of various factors such as wind generator type including Type-III (Doubly Fed Induction Generator, DFIG) and Type-IV (Full Converter, FC), wind generator grid-side converter (GSC) control (coupled/decoupled sequence [14]), Fault-Ride-Through (FRT) function, and wind generation level and capacity to determine the most influential modeling details that a protection engineer should incorporate in such a study. Simulation tests have been carried out on a model of the IEEE PSRC WG-D6 [2] and IEEE PSRC WG-D29 test systems [4] including wind generation within the EMTP [19] software environment.

II. Impact of Wind Generation on Power Swing Protection

To illustrate the impact of wind generation on power swing protection, let us consider the two-machine system of Fig. 1 [2] consisting of two synchronous generators (SGs) represented by voltage sources E_S and E_R behind impedances Z_S and Z_R, a transmission line represented by Z_L, and a distance relay denoted by R. It is assumed that E_S has a phase advance of δ with respect to E_R.

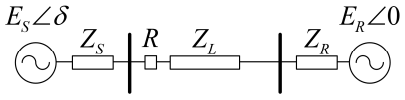

Fig. 1. Two-machine system.

The PSB function of relay R measures the rate of change of the apparent impedance to differentiate between a power swing and a fault [2]. This rate is very fast during a fault since it is predominantly determined by the amount of signal filtering in the relay. By contrast, the rate is slow during a power swing because it is subject to the large inertia of machines. This slow rate can be explained using (1) which presents the impedance measured by the distance relay during a power swing.

$$Z=\frac{Z_S+Z_L+Z_R}{2}\left(1-j\cot\frac{\delta}{2}\right)-Z_S \qquad (1)$$

As (1) shows, the rate of change of Z is proportional to the two-machine slip frequency $d\delta/dt$ which is a function of system inertias. High shares of wind generation lead to the reduction of inertia, faster frequency dynamics, and hence, increased rate of change of Z. The PSB function may fail to detect such faster power swings since PSB settings are determined based on the maximum rate of change of Z under SG [1],[2] which may not be adequate for the successful detection of a potentially faster swing under wind generation.

High shares of wind generation may also result in OST malfunction. The reach of an OST element is determined based on a point along the trajectory of Z where the power system cannot regain stability [1],[2]. Since wind generation alters the trajectory of Z, the reach of the OST element calculated under SG may not be adequate for its proper operation under wind generation.

Further than the impact on the PSB and OST functions, wind generation may also influence the location of the EC which is a point in a power system where voltage becomes zero during an unstable swing [1],[2]. As reference [2] has shown, the location of EC in Fig. 1 is a function of Z_S and Z_R. These impedances may have a different value when the represented source is a wind generator instead of a SG. Hence, high shares of wind generation may necessitate recalculating the location of EC and, thereby, the optimal location for the placement of the OST protection relays.

The next sections present cases of PSB and OST misoperation and the movement of EC under wind generation.

III. Results on the IEEE PSRC D6 Test System

Fig. 2 shows a schematic diagram of the IEEE PSRC WG-D6 test system [2] including wind generation. The test system is a 500-kV transmission system connecting generating stations A and D to an equivalent system denoted by S1 through transmission lines L1-L4. The generating stations A and D incorporate four identical 250-MVA SGs represented by G1-G4 interfaced to the grid through identical transformers Tr1-Tr4. The models of G1-G4 include control schemes employing exciter SEXS, power system stabilizer IEEEST1, and governor IEESGO. S1 models the rest of the transmission system and consists of a 230-kV ideal voltage source and a Thévenin impedance. The power flow is from G1-G4 to S1. The breaker connecting substation E to B is initially open, and the rest of breakers are initially closed.

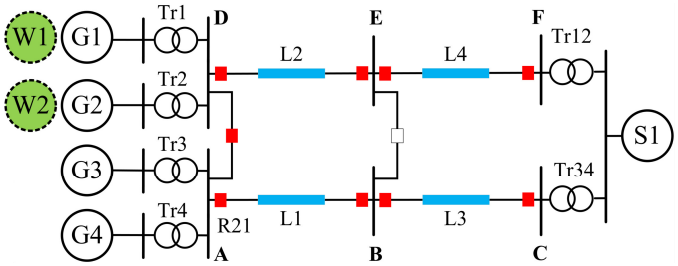

Fig. 2. Schematic diagram of the IEEE PSRC WG-D6 test system [2] including wind generation.

To study the impact of wind generation, SGs G1 and G2 have been replaced by two DFIG-based wind parks denoted by W1 and W2. Reference [6] presents their mathematical model and converter controls, and hence, the detailed model is not presented here. The model of wind parks consists of aggregated models of 1.5-MW DFIG wind turbine units interfaced to the grid through a collector grid and a wind park transformer and a wind park control scheme. The model of each wind turbine consists of mechanical parts, a back-to-back converter represented by an average model, a wind turbine transformer,

and current and dc-voltage control schemes. The GSC control implements both coupled and decoupled sequence control [14] which allows studying their influence on power swing characteristics.

Simulation tests show that a fault on L1 or L2 followed by a loss of the faulted line results in a power swing which can be stable or unstable depending on fault clearing time and pre-fault loading conditions. Longer fault clearing times can be due to a stuck breaker. The power swing is between generators G1-G4 and the rest of the system and is a result of the acceleration of generators during a fault and reduced power transfer capability due to the loss of the faulted line.

The original case [2] does not incorporate power swing protection. This paper adds a multi-function relay denoted by R21 at terminal A incorporating distance and power swing protection functions. The next section presents the settings of this relay.

A. Setting of Distance and Power Swing Protection

Fig. 3 shows the distance relay zones (Z1, Z2, and Z3) and power swing protection elements (outer, middle, and inner elements) of relay R21 on an impedance plane showing the A-to-C interconnection (lines L1 and L3). All impedances have been measured on the secondary side of the current transformer (CT) and voltage transformer (VT) of R21; the CT has a ratio of 800/5A, and the VT has a turns ratio of 500/0.115kV. The settings have been obtained assuming G1-G4 to be connected (no wind generation).

The reach of zone 1, 2, and 3 of the distance relay have been set at 80%, 135%, and 200% of L1, respectively. All three zones are forward zones. Zone 1 is instantaneous, while backup zones 2 and 3 have a time delay of 20 and 40 cycles, respectively.

The power swing function uses a mho-with-blinders detection scheme [1] employing three concentric circles restrained by three sets of blinders to restrict the operation of power swing protection for loads outside of the blinders. The power swing protection supervises all three zones of the distance relay. Its settings have been calculated as follows:

- PSB: the PSB function uses the outer and middle elements separated by an impedance ΔZ together with a timing device to count down a predetermined time delay ΔT as the impedance locus travels between the two elements. If the measured impedance crosses the concentric characteristics before the timer expires, the PSB classifies the event a system fault and does not issue a PSB signal. However, if the timer expires before the measured impedance crosses the concentric characteristics, the PSB declares the event as a power swing and issues a PSB signal to block the distance relay elements operation. The settings of PSB are determined based on the swing impedance trajectory of the most severe stable swing [2] which corresponds to an 88-ms three-phase-to-ground fault on line L2 close to substation E with followed by the outage of lines L2 and L4. Simulation results show that the corresponding maximum anticipated load impedance is 5.575-*j*3.35Ω, the point where the most severe swing reverses direction is at 3.72+*j*3.59Ω, and the time it takes the measured impedance to cross the outer and middle elements is 29 cycles. The outer element should be set such that it does not include the maximum anticipated load impedance of 5.575-*j*3.35Ω. Thus, the reverse reach of the outer mho element has

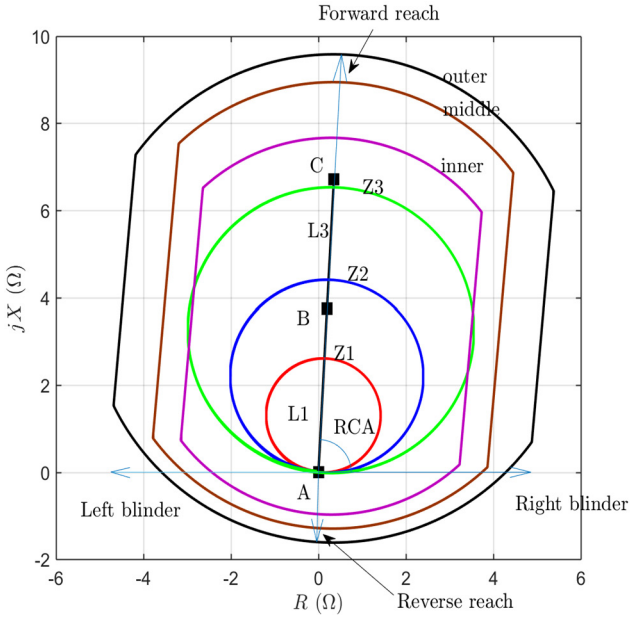

Fig. 3. R-X diagram of A-to-C interconnection showing the zones of distance protection (Z1, Z2, Z3) and the concentric elements of power swing function.

TABLE 1. CALCULATED SETTINGS OF THE DISTANCE AND POWER SWING PROTECTION OF RELAY R21 OF FIG. 2.

Setting	Value	Calculation procedure
Distance Relay		
Z1	3.00Ω	80% of L1
TD1	0 cycles	Time delay of Z1
Z2	5.07Ω	135% of L1
TD2	20 cycles	Time delay of Z2
Z3	7.51Ω	200% of L1
TD3	40 cycles	Time delay of Z3
Power Swing Relay		
Line impedance	3.75Ω ∠87°	Positive sequence
	11.26Ω ∠84°	Zero sequence
Forward reach outer	11Ω	Set to more than the forward reach middle.
Reverse reach outer	1.84Ω	Set to more than the reverse reach middle.
Forward reach middle	10.30Ω	Set to encompass the largest distance protection zone to be blocked by PSB.
Reverse reach middle	1.47Ω	
Forward reach inner	8.83Ω	Set to less than the forward reach middle.
Reverse reach inner	1.10Ω	Set to less than the reverse reach middle.
Forward RCA	87°	Set equal to the phase angle of the positive sequence line impedance.
Reverse RCA	87°	Set the same as forward RCA.
Right blinder outer	5.52Ω	Must be set less than maximum load impedance.
Left blinder outer	5.52Ω	Set same as the right blinder outer.
Right blinder middle	4.42Ω	To encompass the largest distance relay zone to be blocked.
Left blinder middle	4.42Ω	Set same as the right blinder middle.
Right blinder inner	3.68Ω	To ensure that it does not trip for the most severe stable swing.
Left blinder inner	3.68Ω	Set same as the right blinder inner.
PSB time delay	0.048s	Set based on the maximum rate of change of impedance to ensure fastest OOS conditions are detected.
PSB reset delay	0.16s	

been set at 2Ω (less than the absolute imaginary part of the maximum anticipated load impedance) and the resistive reach of outer blinder has been set at 5.52Ω (less than the absolute real part of the maximum anticipated load impedance). The forward reach of the outer mho element has been set at 11Ω. The blinders have been set parallel to the line impedance by setting relay characteristic angle (RCA) at 87°; this optimizes the measurement of delta impedance because the power swing impedance vector normally enters the protection zones at an angle of nearly 90° to the line angle [2]. The middle element should be set such that it encompasses the largest reaching zone of distance element to be blocked which is Z3 with a reach of 7.22Ω. Thus, the forward and reverse reach of the middle mho element have been respectively set at 10Ω and 1.5Ω to put a circle with a diameter of 11.5Ω around Z3 to ensure that it is fully encompassed. The resistive reach of the middle blinder has been set at 4.41Ω to impose a delta impedance of ΔZ=1.1Ω between the outer blinder (5.52Ω) and middle blinder (4.41Ω). The required ΔT to detect the most severe stable swing is less than 29 cycles. A conservative value of ΔT=3 cycles has been selected to ensure that faster OOS conditions are also detected;

- OST: the OST function differentiates between stable and unstable swings using the inner element which is set at a point along the OOS swing trajectory where the power system cannot regain stability [2]. The simulation of the most severe stable swing shows that the OOS point is at 3.72+*j*3.59Ω where swing reverses direction. Thus, the resistive reach of the inner blinder has been set at 3.68Ω (less than the absolute imaginary part of the OOS point) to ensure that the most severe stable swing is not declared an OOS.

The next section studies the efficiency of the calculated settings under wind generation. It should be mentioned that in the simulation tests to follow, the circuit breaker corresponding to relay R21 and the internal protection of the wind generators have been blocked to give a presentation of the full impedance trajectory during all studied contingencies.

B. Impact of Wind Power Integration Level

This section studies three wind integration levels: no wind (when G1-G4 are all connected); 25% wind (when W1 replaces G1); and 50% wind (when W1 and W2 replace G1 and G2). The wind parks supply the same real and reactive power as G1 and G2 in a steady state to ensure that the test system is subjected to the same pre-fault steady-state condition. Rated wind speed condition is considered.

1) Case 1: PSB Misoperation

A 270-ms three-phase-to-ground fault has been applied on line L2 close to substation E followed by the outage of lines L2 and L4 at t=2s resulting in an OOS condition. The event has been simulated under no wind and 25% wind. Fig. 4 depicts the swing impedance trajectory during the first 30 cycles of the power swing, and Fig. 5 shows the response of distance and power swing relays. As Fig. 4 shows, under no wind, the impedance trajectory crosses the outer and middle elements in more than the PSB time delay setting of 3 cycles. Hence, the PSB successfully detects the swing and issues a PSB signal to block zones 1, 2, and 3 of distance protection, as shown in Fig. 5 (PSB). Furthermore, the OST function detects the OOS condition as soon as the swing trajectory enters the inner element and issues an OST signal as shown in Fig. 5 (OST). Zone 2 of distance relay responds to the swing and issues a signal to declare a fault in zone 2 as shown in Fig. 5 (Z2_PKP), nevertheless it is blocked by the PSB. Under 25% wind, the impedance trajectory crosses the outer and middle elements in about 2 cycles which is less than the PSB time delay setting. Hence, the power swing protection fails to detect the power swing and does not issue the PSB signal as shown in Fig. 5 (PSB). As the swing continues, the impedance trajectory enters zone 2 of the distance relay, and the power swing is mistakenly declared as a fault in zone 2 which is picked up by zone 2 of the distance protection as shown in Fig. 5 (Z2_PKP). This could result in undesired instantaneous tripping of line L1 if zone 2 is used in a pilot relaying scheme such as Permissive Overreaching Transfer Trip (POTT). Fig. 4 further shows that the impedance trajectory travels a longer distance under 25% wind during the same time interval due to the increased rate which is consistent with the conclusion of Section II.

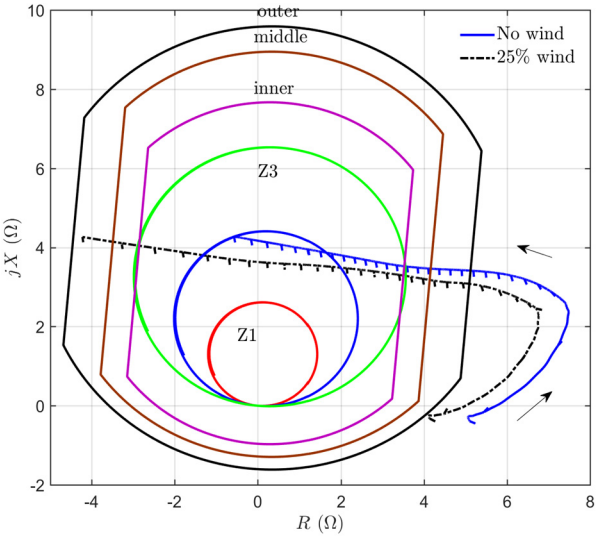

Fig. 4. Swing impedance trajectory under no wind (blue) and 25% wind generation (dashed black) for the PSB misoperation case of Section III.B.1).

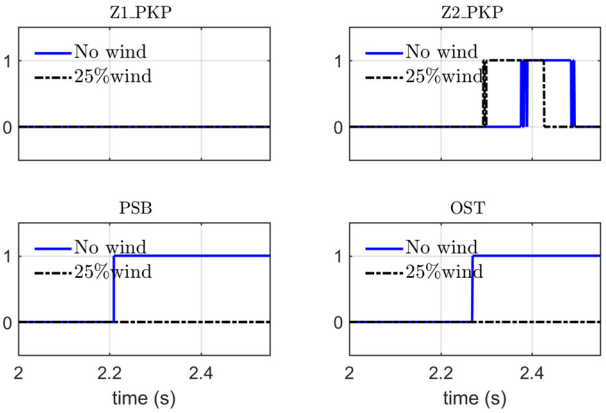

Fig. 5. Distance and power swing relay signals under no wind (blue) and 25% wind (dashed black) for the PSB misoperation case study of Section III.B.1): distance relay zone 1 pick-up signal (Z1_PKP); distance relay zone 2 pick-up signal (Z2_PKP); power swing PSB signal (PSB); and power swing OST signal (OST).

Possible solution—The above case study illustrates that high shares of wind integration may increase the rate of change of the swing impedance vector and cause PSB misoperation. To avoid such misoperation, a solution is to reduce the PSB time delay by recalculating the maximum rate of impedance change under wind generation. For the reported case study, conducted simulation tests show that reducing the PSB time delay from 0.048s to 0.016s fixes the PSB misoperation problem for both 25% and 50% wind integration levels. It should be mentioned that reducing the PSB time delay does not compromise the detection of power swing under SG where slower power swings are expected. Nevertheless, special care needs to be taken when reducing the PSB time delay since an excessively small PSB time delay may cause the PSB function to mistake a fault for a power swing and unintentionally block distance protection elements during the fault. For the test system of this paper, the modified PSB time delay of 0.016s did not cause such misoperation problem since the rate of change of fault impedance was much faster.

2) Case 2: OST Malfunction

This case study compares the most severe stable swing under no wind and 50% wind generation. Under no wind, the most severe stable swing is caused by an 88-ms three-phase-to-ground fault on line L2 close to substation E followed by the outage of lines L2 and L4. Under 50% wind, the most severe stable swing corresponds to a 120-ms three-phase-to-ground fault on line L2 close to substation E resulting in the loss of L2 and L4. Fig. 6 depicts the swing impedance trajectory of the most severe stable swing under no wind and 50% wind, and Fig. 7 shows the response of power swing protection. As Fig. 6 shows, under no wind generation the impedance trajectory reverses direction at 3.72+j3.59Ω which is outside the inner element. Hence, the power swing protection declares the swing as stable, issues a PSB signal as shown in Fig. 7 (PSB), and does not issue an OST signal as shown in Fig. 7 (OST). However, under 50% wind the impedance trajectory reverses direction at 3.16+j3.15Ω which falls inside the inner element. Thus, the relay mistakenly declares an OOS condition and issues an OST signal as shown in Fig. 7 (OST).

Possible solution—To prevent such an OST malfunction, a solution is to revise the reach of the inner element such that the most severe stable swing under wind generation does not enter the inner element. This requires extensive simulation studies including wind generation under different operating conditions. Conducted simulation tests show that the OST malfunction can be fixed by reducing the resistive reach of the inner blinder from 3.68Ω to 2.9Ω.

3) Case 3: Movement of EC

To show the movement of EC as a function of wind generation level, an OOS condition has been simulated under no wind, 25% wind, and 50% wind. The OOS is caused by a three-phase-to-ground fault on line L2 followed by the outage of L2 and L4. The location of EC is calculated using the method of [2] by plotting the swing locus superimposed on transmission lines L1 and L3 to determine which line the swing locus goes through. Fig. 8 shows the results. As shown, under no wind, the location of EC is at 0.22+*j*4.18Ω, and the swing locus passes through line L3. Hence, the optimal location to implement the OST function is line L3. Nevertheless, under 25% and 50% wind integration, the EC moves to 0.20+*j*3.76Ω and 0.14+*j*2.59Ω on the impedance plane, respectively, and the locus passes through line L1. Therefore, line L1 is the optimal location to implement the OST function under 25% and 50% wind. This case study shows that it is necessary to recalculate the location of EC when wind generators are connected to ensure that the OST function is implemented in the optimal location.

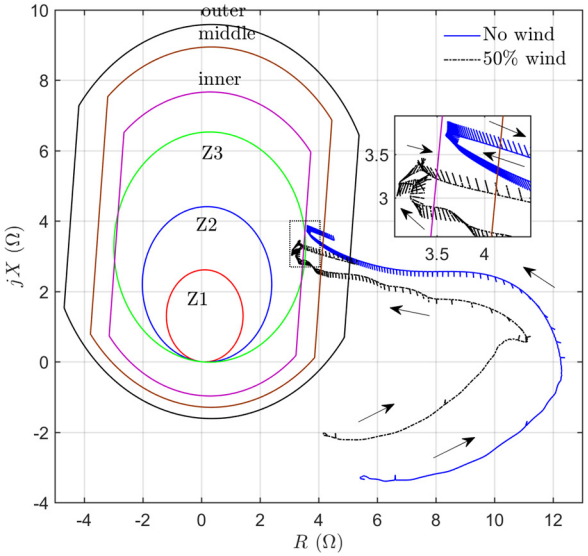

Fig. 6. Swing impedance trajectory of the most severe stable swing under no wind (blue) and 50% wind generation (dashed black) for the OST malfunction case of Section III.B.2).

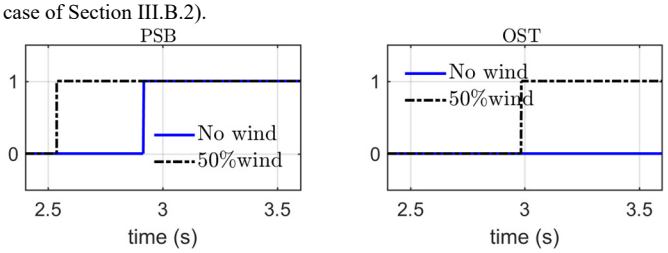

Fig. 7. Power swing relay signals under no wind (blue) and 50% wind generation (dashed black) for the OST misoperation case study of Section III.B.2): power swing PSB signal (PSB); and power swing OST signal (OST).

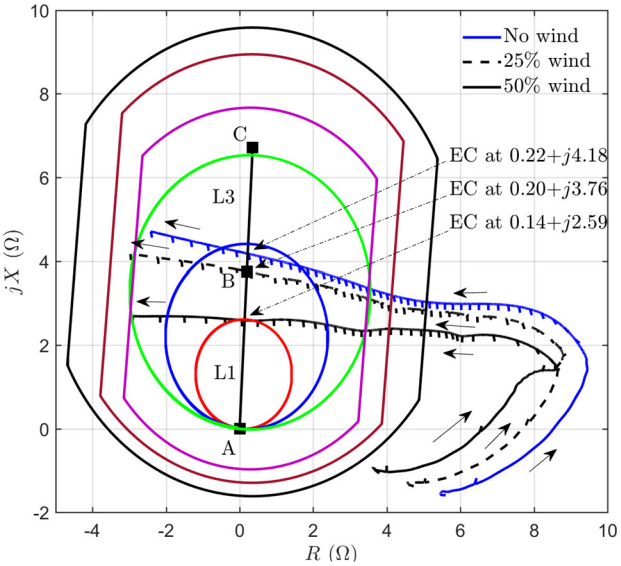

Fig. 8. The movement of EC of the IEEE PSRC D6 test system as a function of wind integration level, case study of Section III.B.3).

IV. Results on the IEEE PSRC D29 Test System

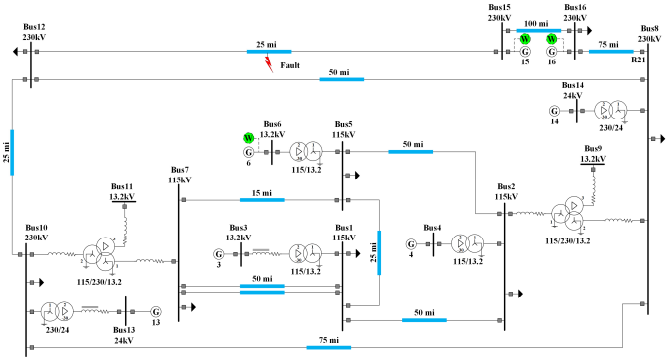

Fig. 9. Schematic diagram of the IEEE PSRC D29 test system [4] with SGs on buses Bus6, Bus15, and Bus16 replaced by wind parks.

To further illustrate the misoperation of power swing protection due to wind generation, this section provides examples of PSB and OST misoperation in the IEEE PSRC WG D29 test system [4] including wind generation. Fig. 9 shows the schematic diagram of this test system. The original IEEE PSRC WG-D29 case [4] provides power swing protection data assuming SG. The objective of this section is to study the adequacy of these settings under wind generation. To that end, SGs on buses Bus6, Bus15, and Bus16 have been replaced by Type-III wind parks whose models are the same as those of Section III. This introduces approximately 1000MW wind generation into the test system which amounts to nearly 50% of the total generation.

A. *Case 1) PSB Misoperation*

A 150-ms three-phase-to-ground fault is applied on the line connecting Bus12 to Bus15 followed by the outage of the line resulting in a power swing. The simulation results are obtained from a multifunctional relay denoted by R21 located at Bus8 including distance and power swing protections. The original PSB time delay of R21 is 2 cycles [4]. Fig. 10 and Fig. 11 present the results under SG and 50% wind generation, showing the same PSB misoperation issue as that of Section III.B.1). Under 50% wind, the power swing results in an OOS condition, the impedance trajectory crosses the outer and inner elements in about 1.8 cycles which is less than the PSB time delay, the relay mistakenly classifies the event as a fault, and PSB is not issued as shown in Fig. 11 (PSB). This misoperation problem can be fixed by reducing the PSB time delay from 2 cycles to 1 cycle. The results of this case study further verify the conclusion of this paper that increased wind integration level increases the likelihood of PSB misoperation.

B. *Case 2) OST Malfunction*

This case study shows the most severe stable swing under SG and wind generation which is respectively caused by a 30-ms and 150-ms three-phase-to-ground fault on the line connecting Bus12 to Bus15 followed by the outage of the line. Fig. 12 compares the swing impedance trajectory, and Fig. 13 shows the response of the power swing protection. As shown, the PSB function successfully detects the swing; however, under wind generation (dashed black) the impedance trajectory crosses the inner element and the OST function mistakenly issues an OST signal declaring an OOS condition. This case study shows that the original OST settings obtained under SG are not adequate for a proper OOS detection under wind generation.

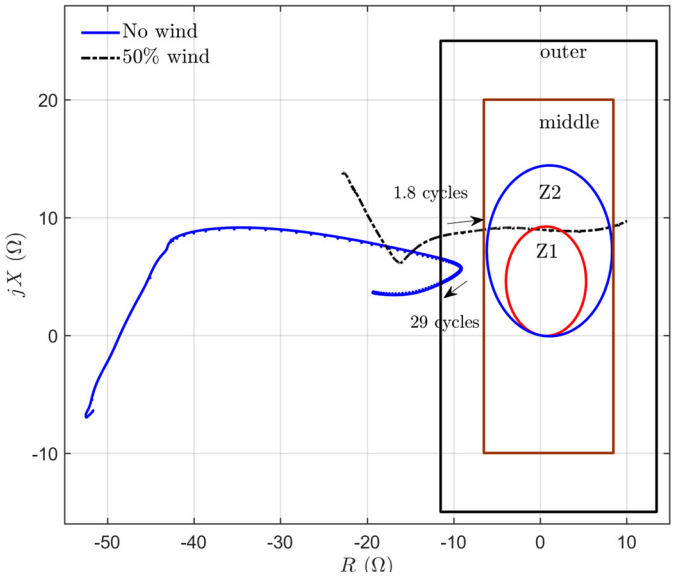

Fig. 10. PSB misoperation case in the IEEE PSRC D29 test system: swing impedance trajectory under no wind (blue) and 50% wind (dashed black).

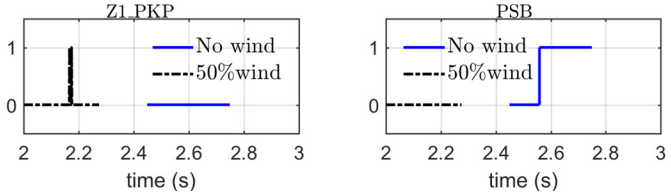

Fig. 11. Power swing relay signals under no wind (blue) and 50% wind generation (dashed black) for the PSB misoperation case study of Section IV.A.

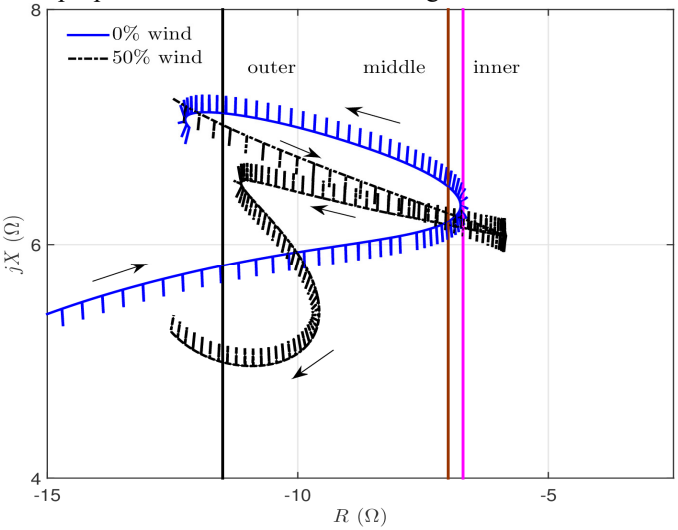

Fig. 12. Swing trajectory of the most severe stable swing under no wind (blue) and 50% wind (dashed black); the OST malfunction case of Section IV.B.

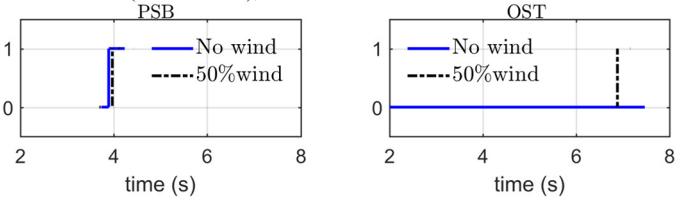

Fig. 13. Power swing relay signals under no wind (blue) and 50% wind generation (dashed black) for the OST misoperation case study of Section IV.B: power swing PSB and OST signals.

V. Impact of Wind Generator Characteristics

Studying the impact of wind generation on power swing protection entails simulation studies incorporating adequate features of a wind generator. The objective of this section is to determine key details that influence power swing characteristics under wind generation and hence should be incorporated in such a study.

A. *Wind Park Size and Operating Conditions*

The impact of wind power integration level is demonstrated in Section III.B for rated wind speed. Similar observations can be made for reduced wind power generation scenarios due to wind turbine outages. Slow wind speeds also cause reduced wind power generation and its impact is studied on IEEE PSRC D6 test system considering three cases where both W1 and W2 have 250 MW, 500 MW and 1000 MW installed capacities. In all cases, W1 and W2 produce 220 MW. The corresponding wind speeds are 11.24m/s, 9m/s, and 7.2m/s, respectively.

Fig. 14 shows the swing impedance trajectory for the first 60 cycles for the simulated installed capacities. Despite the same power outputs, the wind generation installed capacity affects both the rate of change of the impedance vector and the swing pattern which may impact the operation of both PSB and OST.

Conducted simulation tests showed that decreased wind generation capacity results in faster swings under 25% and 50% wind integration levels which makes PSB misoperation more likely (see Section III.B). Nevertheless, in a number of other cases the decreased capacity resulted in slower swings making PSB misoperation less likely. Therefore, no definitive conclusion could be made regarding the impact of wind generation capacity on the likelihood of PSB misoperation. However, given the impact on the rate of change of swing impedance, it is recommended to consider the wind generation capacity in the calculation of the settings of the PSB function.

Conducted simulation tests further demonstrated that the wind park size and operating conditions impact the trajectory of the most severe stable swing and, therefore, may impact the operation of the OST function. Despite the same power generation (220 MW), the OST misoperation occurred at 250 MW wind park but not at 500 MW and 1000 MW wind parks. Due to this impact, it is recommended to consider different wind speed and wind turbine outage scenarios in the calculation of the settings of the OST function.

Wind park size also impacts the location of EC. Fig. 15 shows the movement of the EC due to wind generation at 50% of rated power. The comparison of Fig. 8 and Fig. 15 reveals that wind generation capacity impacts the movement of EC.

B. *Wind Generator Type*

Fig. 16 compares the swing impedance trajectory for the first 10 cycles of a power swing in the IEEE PSRC D29 test system under wind generator Type-III and Type-IV (assuming a GSC control rise-time of 10ms). As shown, the starting point of swing is the same for the two cases since the wind generators supply the same real and reactive powers prior to the swing. Nevertheless, the trajectory exhibits considerable differences due to different control of Type-III and Type-IV generators.

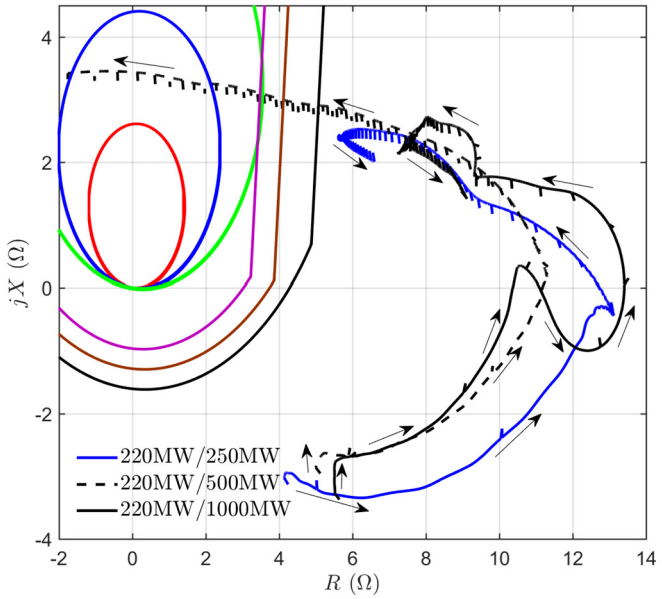

Fig. 14. Swing impedance trajectory versus various installed wind generation capacity (IEEE PSRC D6).

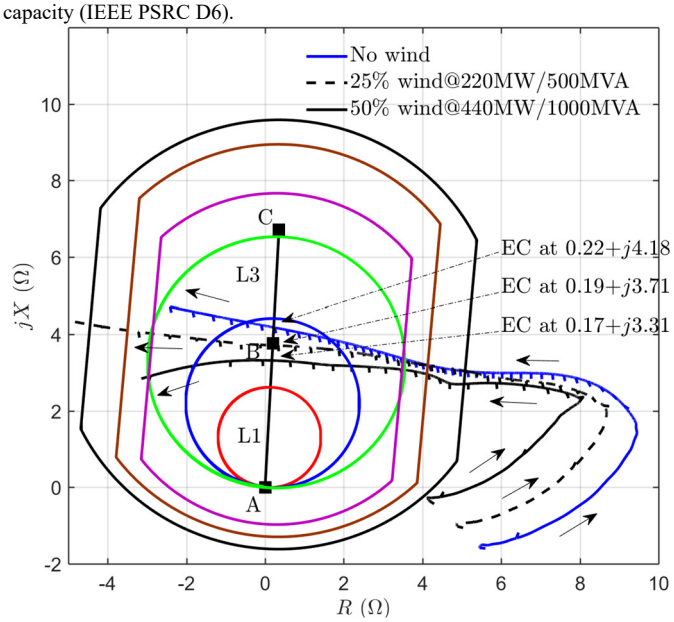

Fig. 15. Movement of EC due to wind generation at 50% wind generation capacity (IEEE PSRC D6).

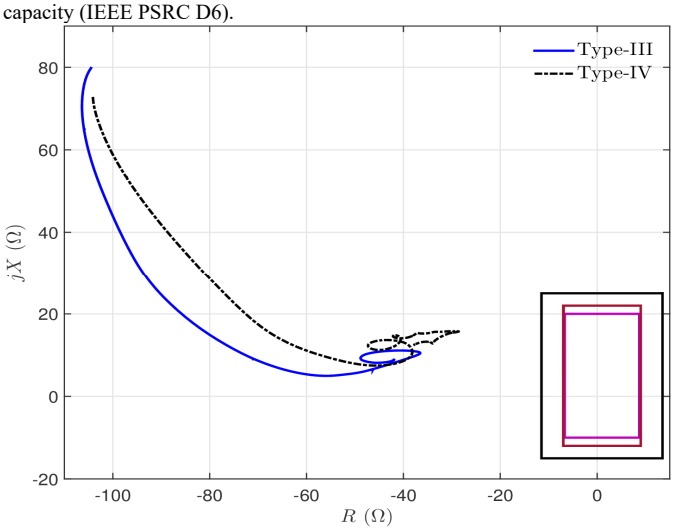

Fig. 16. Comparison of swing impedance trajectory under Type-III (blue) and Type-IV (dashed black) wind generators (IEEE PSRC D29).

Fig. 17 compares an example swing impedance trajectory under Type-III and Type-IV assuming 25% wind integration level. The results suggest a difference in the rate of change of swing impedance due to the type of wind generator; under Type-III, the swing crosses the outer and middle element in about 9.2 cycles compared to 12 cycles under Type-IV which suggests that wind generator type may impact the operation of PSB. Fig. 17 further shows that the swing locus passes through line L3 at 0.21+*j*4.08Ω under Type-III compared to 0.22+*j*4.19Ω under Type-IV. Hence, in this case the type of wind generator has an insignificant impact on the location of EC. Fig. 18 compares the most severe stable swing impedance trajectory assuming 25% wind integration level. Under Type-III, the swing reverses direction at 3.77+*j*3.54 Ω compared to 4.05+*j*3.34 Ω under Type-IV suggesting that the type of wind generator may impact the OST function.

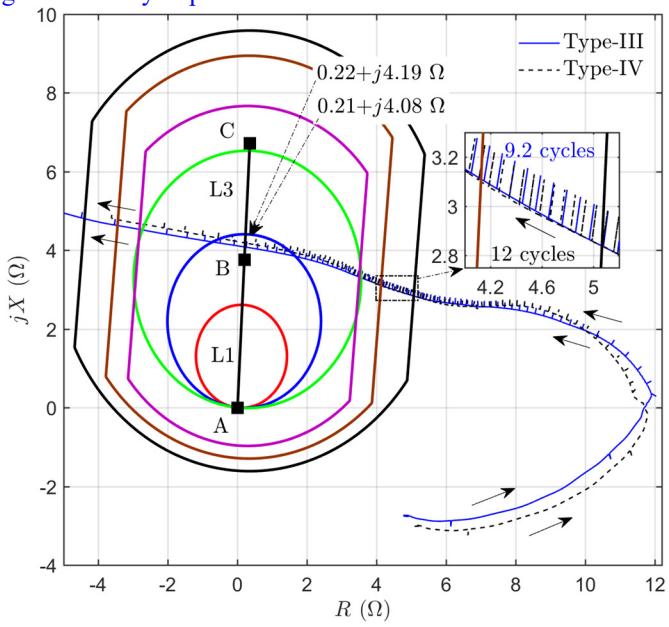

Fig. 17. Example unstable swing impedance trajectory under Type-III and Type-IV assuming 25% wind integration level (IEEE PSRC D6 system).

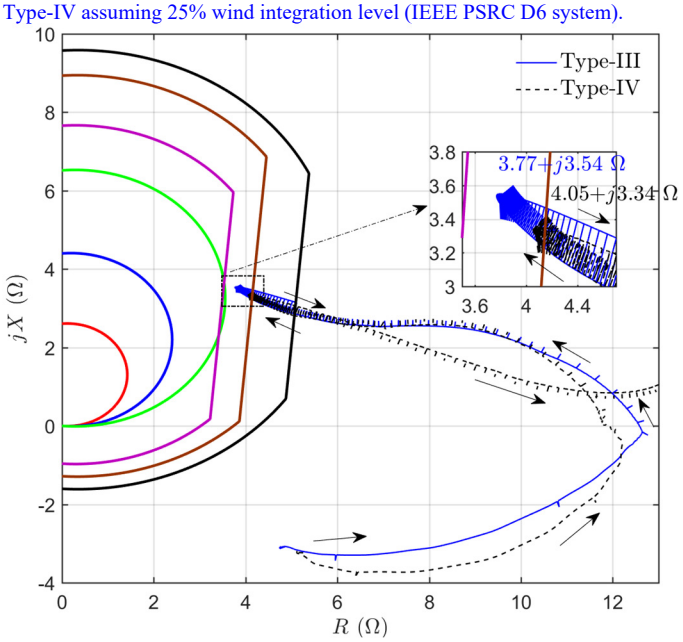

Fig. 18. The most severe stable swing impedance trajectory under Type-III and Type-IV assuming 25% wind integration level (IEEE PSRC D6 system).

This case shows that wind generation type should be included in a power swing protection study due to its impact on swing characteristics. Conducted simulation tests show that the PSB and OST misoperation of Sections III and IV occur under both Type-III and Type-IV.

C. GSC Control

Fig. 19 compares the impedance trajectory of a power swing in the IEEE PSRC D29 test system under GSC coupled and decoupled sequence control in Type-III and Type-IV wind generators. As shown, in Type-III, the GSC control does not have a significant impact, whereas in Type-IV, the impact is more considerable. The reason is that in Type-IV, the power converter contributes 100% of the generator rating, and therefore, GSC control has a more appreciable influence on the dynamic characteristics compared to Type-3 where the power converter contributes only part of the generator rating. This study shows that GSC control may have a considerable impact on power swing characteristics under wind generation and hence should be considered in a power swing simulation study.

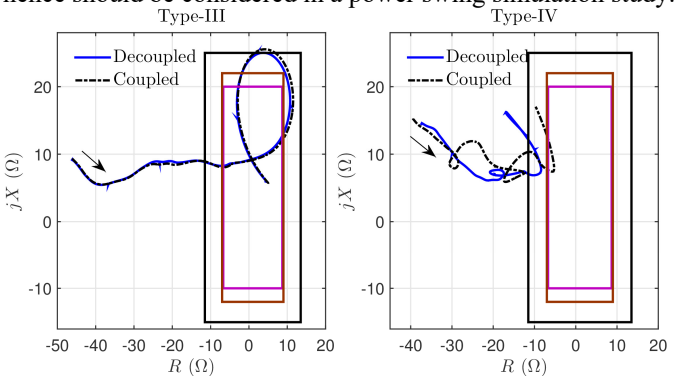

Fig. 19. Comparison of swing impedance trajectory under decoupled sequence (blue) and coupled sequence control (dashed black) in Type-III (left) and Type-IV (right) wind generators (IEEE PSRC D29).

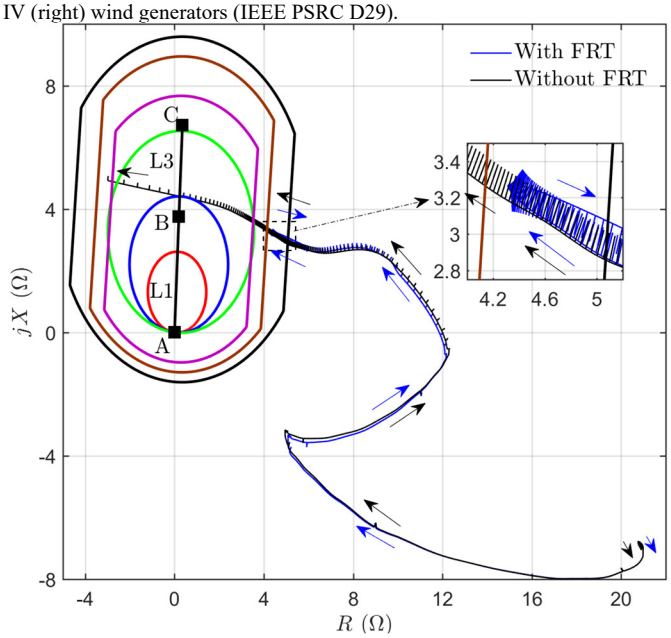

Fig. 20. Comparison of swing impedance trajectory with and without FRT (IEEE PSRC D6 system).

The FRT requirement in grid codes (such as [20]) defines the reactive output current of the converter-interfaced renewable during voltage disturbances. The FRT operation is essential to

enhance the stability margin of the power system. When FRT function is deactivated, the reactive power support is limited. Fig. 20 compares swing impedance trajectory for the same fault event under wind generator Type-IV with and without FRT functions (blue and black, respectively). The swing becomes unstable when the FRT function is deactivated. For this specific case, the FRT function has an indirect, but a significant impact on swing characteristic. On the other hand, the impact of FRT function on swing characteristic is not significant when the system remains stable after deactivating the FRT function of the wind generator.

VI. Conclusion

This paper has investigated the impact of wind generation on power swing protection and provided possible solutions to ensure the efficiency of protection under high shares of wind generation. It is demonstrated that the likelihood of PSB misoperation increases with increased wind generation. In that case the PSB time delay setting needs to be revised after identifying the fastest power swing. The wind generation also changes the swing impedance trajectory and hence has an impact on OST function. The reach of the inner element needs to be revised to make sure that the most severe but stable power swing does not enter the inner element. The location of EC may also change as the level of wind generation increases. It is important to re-calculate its location. The capacity, type, GSC control options (decoupled vs. coupled), and FRT function are among the key factors that need to be considered in protection studies as they all influence the level of impact on PSB and OST functions in addition to the location of EC.

Fig. 21 presents the proposed steps to re-tune the settings of power swing protection in presence of wind generation. The first step is to re-calculate the EC to determine the optimal location for the implementation of the OST protection. The important parameters that should be incorporated in this step are wind integration share and wind park size and operating conditions. The next step is to find the fastest power swing considering wind generation share and type, wind park size and operating conditions, wind speed, and GSC control. If the existing PSB time-delay setting is not small enough to detect this fastest swing, the PSB time-delay should be reduced. The final step is to find the most severe stable power swing by considering the impact of wind generation share and type, wind park size and operating conditions, wind speed, and GSC control. If this most severe stable swing crosses the inner element, the resistive reach of the element should be reduced.

VII. Appendix: Wind Turbine Generator Model

This paper used the detailed generic electromagnetic transient (EMT) models of Type-III and Type-IV wind turbine generators (WTGs) in [21]. This part presents Type-IV WTG control system briefly to clarify the terms FRT operation and decoupled sequence control (DSC). The utilized model of Type-III WTG has the same level of details, but is not presented here due to space limitations. Reader should refer to [21] for further details of Type-IV WTG controls. All details for the Type-III WTG controls can be also found in [21].

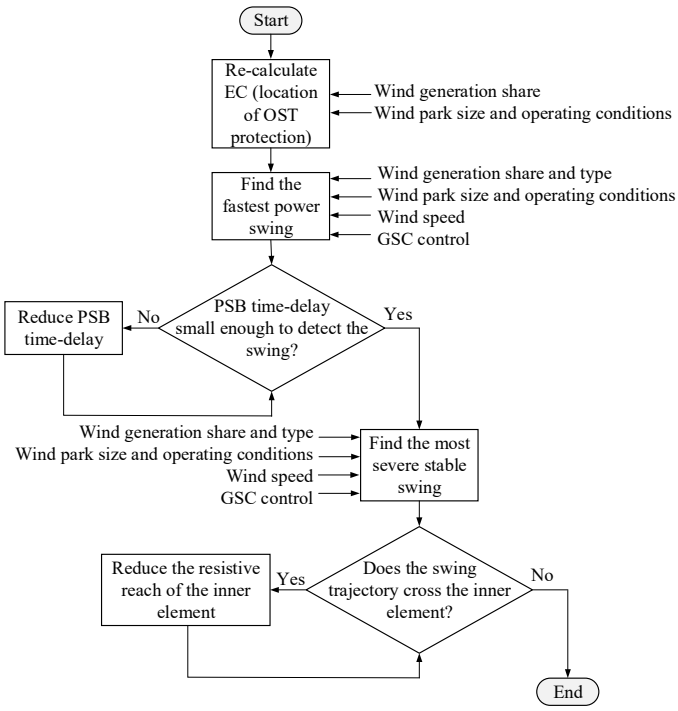

Fig. 21. Proposed steps to re-tune the settings of power swing protection in presence of wind generation.

The considered Type-IV WTG topology in [21] uses a permanent magnet synchronous generator (PMSG) and an ac-dc-ac converter system consisting of two PWM voltage source converters: stator side converter (SSC) and grid side converter (GSC). The dc resistive chopper is used for the dc bus overvoltage protection. A line inductor (choke filter) and an ac harmonic filter are used at the GSC to improve the power quality. The WTG is connected to a medium voltage (MV) collector grid through a transformer.

Both SSC and GSC are controlled by a two-level controller. The slow outer control calculates the reference dq-frame currents and the fast inner control allows controlling the converter ac voltage reference. SSC operates at unity power factor and controls the PMSG torque to follow the reference given by a Maximum Power Point Tracking (MPPT) algorithm for optimal power generation depending on wind speed.

The schematic diagram of GSC control is shown in Fig. 22. GSC operates in the voltage reference frame. d-axis current of GSC (i_{dg}) is used to control dc bus voltage (V_{dc}). q-axis current of GSC (i_{qg}) is used to control the positive sequence terminal voltage of GSC ($\left|\overline{V}_g^+\right|$). The voltage reference (V') is adjusted by the proportional-integral (PI) reactive power regulator of the wind park controller (WPC) to achieve the desired reactive power at the point of interconnection (POI).

During normal operation, the priority is given to the active power component of the GSC currents, i.e.

$$\begin{aligned} i'_{dg} &< I_{dg}^{\lim} && , I_{dg}^{\lim} = 1\ pu \\ i'_{qg} &< I_{qg}^{\lim} = \sqrt{\left(I_g^{\lim}\right)^2 - \left(i'_{dg}\right)^2} && , I_g^{\lim} = 1.1\ pu \end{aligned} \tag{2}$$

where $I_g^{\lim}$ is the GSC current limit.

In this section, all variables are in pu and primed variables

are used to indicate the reference values coming from the controllers. The plus and minus signs ("+" and "-") indicate positive and negative sequence components, respectively.

The grid code requirements, such as [20], include the WTG transient response against severe voltage disturbances. To comply with the requirement in [20], the GSC controller gives priority to the reactive current by reversing the d- and q-axis current limits given (2) during FRT operation.

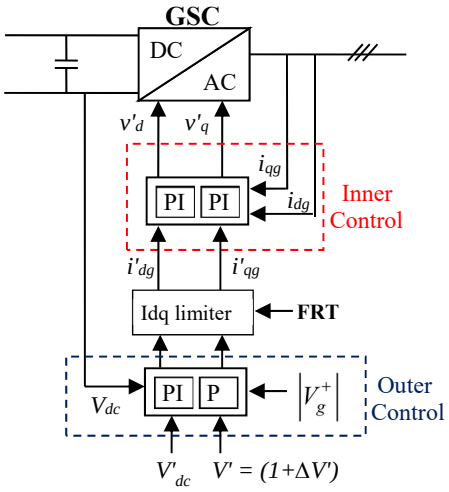

Fig. 22. Schematic diagram of GSC coupled sequence control.

Ideally, the GSC control presented in Fig. 22 is not expected to inject any negative sequence currents to the grid during unbalanced loading conditions or faults. On the other hand, the GSC terminal voltage contains negative sequence components. This causes second harmonic pulsations in GSC power output and dc bus voltage. The elimination of these second harmonic pulsations can be achieved using DSC. As i_{dg}^{+}, i_{qg}^{+}, i_{dg}^{-} and i_{qg}^{-} are controlled, DSC contains four PI regulators as shown in Fig. 23. During normal operation (under unbalanced conditions), the elimination of GSC second harmonic power pulsations is achieved at the expense of reduced reactive power generation (or reserve). On the other hand, the elimination of these power pulsations is achieved at the expense of reduced active power injection of GSC (depending on severity of the voltage sag and wind speed) during FRT operation.

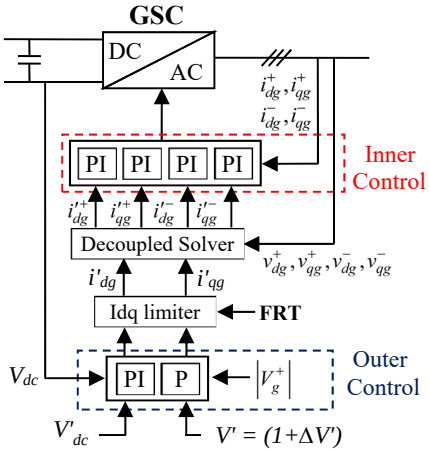

Fig. 23. Schematic diagram of GSC coupled sequence control.

REFERENCES

[1] NERC, "Protection system response to power swings," NERC System Protection and Control Subcommittee Report, Atlanta, GA, Aug. 2013.

[2] IEEE PSRC WG-D6, "Power swing and out-of-step considerations on transmission lines," Jul. 2005.

[3] D. A. Tziouvaras and D. Hou, "Out-of-step protection fundamentals and advancements," *Proceedings of the 30th Annual Western Protective Relay Conference*, Spokane, WA, Oct. 2003.

[4] "Tutorial on Setting Impedance-Based Power Swing Blocking and Out-of-Step Tripping Functions on Transmission Lines", IEEE PSRC WG-D29 Draft Report.

[5] "Impact of Inverter Based Generation on Bulk Power System Dynamics and Short-Circuit Performance", PES-TR68, prepared by the IEEE/NERC Task Force on Short-Circuit and System Performance Impact of Inverter Based Generation, Jul. 2018

[6] R. J. Nelson and H.Ma, "Short circuit contributions of full-converter wind turbines," *IEEE PES T&D Conference*, Orlando, FL, USA, May 2012.

[7] T. Kauffmann, U. Karaagac, I. Kocar, S. Jensen, J. Mahseredjian, and E. Farantatos, "An accurate type III wind turbine generator short circuit model for protection applications," *IEEE Trans. Power Del.*, vol. 32, no. 6, Dec. 2017.

[8] J. Morren and S. W. H. de Haan, "Short-circuit current of wind turbines with doubly fed induction generator," IEEE Trans. Energy Convers., vol. 22, no. 1, pp. 175–180, Mar. 2007.

[9] A. Hooshyar, M. A. Azzouz, and E. F. El-Saadany, "Distance protection of lines connected to induction generator-based windfarms during balance faults," *IEEE Trans. Sustain. Energy*, vol. 5, no. 4, pp. 1193–1203, Oct. 2014.

[10] A. Hooshyar, M. A. Azzouz, and E. F. El-Saadany, "Distance protection of lines emanating from full-scale converter-interfaced renewable energy power plants–Part I: Problem statement," *IEEE Trans. Power Del.*, vol. 30, no. 4, pp. 1770–1780, Aug. 2015.

[11] A. Hooshyar, M. A. Azzouz, and E. F. El-Saadany, "Distance protection of lines emanating from full-scale converter-interfaced renewable energy power plants – Part II: Solution description and evaluation," *IEEE Trans. Power Del.*, vol. 30, no. 4, pp. 1781–1791, Aug. 2015.

[12] L. He, C. C. Liu, A. Pitto, and D. Cirio, "Distance protection of AC grid with HVDC-connected offshore wind generators," *IEEE Trans. Power Del.*, vol. 29, no. 2, pp. 493–501, Apr. 2014.

[13] S. Srivastava, A. Biswal, S. Ganesan, and U. J. Shenoy, "Behavior of self-polarized Mho characteristic on lines fed from DFIG based wind farms," *IEEE Innovative Smart Grid Technologies-Asia*, Bangalore, Nov. 10–13, 2013.

[14] M. Nagpal and C. Henville, "Impact of Power-Electronic Sources on Transmission Line Ground Fault Protection", *IEEE Trans. Power Del.*, vol. 33, no. 1, pp. 62–70, Feb. 2018.

[15] I. Erlich, T. Neumann, F. Shewarega, P. Schegner, and J. Meyer, "Wind turbine negative sequence current control and its effect on power system protection,", *IEEE Power Energy Soc. Gen. Meeting*, Jul. 2013.

[16] R. Teodorescu, M. Liserre, P. Rodriguez, *Grid Converters for Photovoltaic and Wind Power Systems*, 2011, IEEE/Wiley.

[17] J. G. Slootweg and W. L. Kling, "The impact of large scale wind power generation on power system oscillations," *Electrical Power System Research*, vol. 67, no. 1, pp. 9–20, 2003.

[18] D. Gautam, V. Vittal, and T. Harbour, "Impact of increased penetration of DFIG-based wind turbine generators on transient and small signal stability of power systems," *IEEE Trans. Power Syst.*, vol. 24, no. 3, pp. 1426–1434, Aug. 2009.

[19] J. Mahseredjian, S. Dennetière, L. Dubé, B. Khodabakhchian and L. Gérin-Lajoie, "On a new approach for the simulation of transients in power systems," *Electric Power Systems Research*, vol. 77, no. 11, pp. 1514–1520, Sep. 2007.

[20] "Grid code - high and extra high voltage," E.ON Netz GmbH, Bayreuth, Germany, April 2006.

[21] U. Karaagac, J. Mahseredjian, H. Gras, H. Saad, J. Peralta and L. D. Bellomo, "Simulation models for wind parks with variable speed wind turbines in EMTP," research report, Montréal Polytechnique, March 2017.